Uludağ University Journal of The Faculty of Engineering, Vol. 21, No. 1, 2016 RESEARCH

DOI: 10.17482/uujfe.67205

ANALYSIS OF MATERIAL POSITION AND SIZE IN A WAVEGUIDE FED RESONATOR

***Okan SÜLE**[*]*
***Sedef KENT**[**]*

Received: 02.07.2015; accepted: 09.02.2016

Abstract: The main factors that affect electric field distribution, and therefore heat distribution, are the dimensions of the resonator, heating frequency, shape and dielectric properties of the material to be heated, position of the material to be heated within the resonator and the position of the feed guide on the resonator. From among these factors that directly affect heating, this work examined the material thickness. The purpose of this study was to determine the material thickness that will minimise the reflection coefficient. The accuracy of the results obtained by means of the mode matching method was demonstrated by comparing those results with the results obtained through Ansoft's High Frequency Structure Simulator.

Keywords: Mode Matching Method, Reflection Coefficient, Resonator.

Dalgakılavuzu ile Beslenen Bir Rezonatörde Malzeme Konumunun ve Büyüklüğünün Analizi

Öz: Bir mikrodalga rezonatöründe elektrik alan dağılımını dolayısıyla ısı dağılımını etkileyen temel faktörler, rezonatörün boyutları, ısıtma frekansı, ısıtılacak malzemenin şekli ve dielektrik özellikleri, ısıtılacak malzemenin fırın içindeki konumu, besleme kılavuzunun rezonatör üzerindeki konumu şeklinde sıralanabilir. Bu çalışmada ısıtmaya direk etki eden bu faktörlerden malzeme kalınlığı incelenmiştir. Çalışmanın amacı yansıma katsayısını minimize edecek malzeme kalınlığının bulunmasıdır. Mod denkleştirme yöntemiyle bulunan sonuçların doğruluğu Ansoft HFSS ile elde edilen sonuçlarla karşılaştırılarak ispatlanmıştır.

Anahtar Kelimeler: Mod Denkleştirme Yöntemi, Yansıma Katsayısı, Rezonatör

1. INTRODUCTION

Today, there are many papers being published on microwave heating, the use of which is very common (Jia, 1993, Liu et. al., 1994, Iskander et. al., 1994, Zhao and Turner, 1996, Dibben and Metaxas, 1996, Sunberg et. al., 1996, Liu et. al., 1996, Reader and Chan, 1998, Hallac and Metaxas, 2003).

* Uludağ University, Faculty of Engineering, Dept. of Electrical-Electronics Engineering, Gorukle 16059, Bursa.
**Istanbul Technical University, Dept. of Electronics and Communication Engineering, 34469,Istanbul.
Corresponding Author: Okan Süle (osule@uludag.edu.tr)

In the results obtained through the numerical or analytical methods used in these papers, the amplitudes of the reflection coefficients were generally obtained as a function of the

frequency (Requena-Perez et. al., 2004, Monzo´-Cabrera et. al., 2004, Plaza-González et. al., 2005, Pedreno-Molina et. al., 2006, Süle and Kent, 2010). In the present study, however, the effect of material thickness, a component that has not been thoroughly examined, on the variation of the reflection coefficient was examined. In the analysis, the position in which the reflection coefficient is

minimised and the thickness of the material were determined by holding the resonator dimensions, feed position, and operating frequency fixed and varying the material thickness.

There are two primary innovations that are introduced with the conducted analysis. While the first of these is the obtainment of the reflection coefficient on the basis of material thickness, the second is the fact that results were obtained in a short period of time. As it is necessary with the use of Ansoft HFSS, which works on the basis of Finite Element Method (FEM) and was used in this study, or Finite Difference Time Domain (FDTD) method to make a new model for each position and thickness value of the material, obtaining the reflection coefficient takes a very long time. Yet, by means of the position and thickness information that can be defined as variables in the algorithm through the mode matching method in this study, the variation of the reflection coefficient according to the position and thickness of the material can be obtained in a very short period of time and with a high level of accuracy.

2. FORMULATION

We can divide the resonator into four basic parts as shown in Figure 1.

The variable c_1 is the starting point of the feeding guide's x coordinate, and c_2 is the last point of the feeding guide's x coordinate. In the same way, v_1 is the starting point of the feeding guide's y coordinate, and v_2 is the last point of the feeding guide's y coordinate. The variable t is the slab thickness and, d and l are the empty spaces of the resonator. The variables a and b are, respectively, the resonator's x and y dimensions.

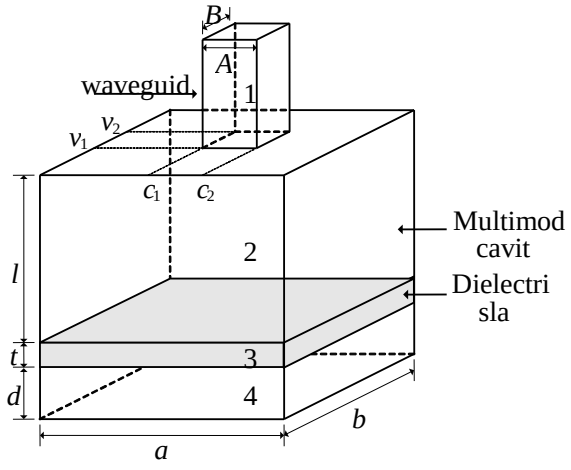

Figure 1:
Three dimensional rectangular cavity loaded with lossy slab

When the basic equalities are taken into account and the equality of the tangential electric field compounds on the point of the first and the second area intersection on the aperture and mode matching equalities in the related boundaries are used, the equation for the electric field can be formed as follows:

$$\vec{E}_s = \vec{e}^{\,h}_{t,10} e^{-jk_{z,10}z} \tag{1}$$

$$\vec{E}_t^{\,I} = \sum_{m=0}^{M}\sum_{n=0}^{N}\left[\begin{array}{l}\left(A_{mn}^{h}e^{+jk_{z,mn}^{I}z} + \delta_{mn,10}e^{-jk_{z,mn}^{I}z}\right)\vec{e}_{t,mn}^{\,h(I)} \\ +A_{mn}^{e}\vec{e}_{t,mn}^{\,e(I)}e^{+jk_{z,mn}^{I}z}\end{array}\right] \tag{2}$$

$$\vec{H}_t^{\,I} = \sum_{m=0}^{M}\sum_{n=0}^{N}\left[\begin{array}{l}\left(A_{mn}^{h}e^{+jk_{z,mn}^{I}z} - \delta_{mn,10}e^{-jk_{z,10}^{I}z}\right)\vec{h}_{t,mn}^{\,h(I)} \\ +A_{mn}^{e}\vec{h}_{t,mn}^{\,e(I)}e^{+jk_{z,mn}^{I}z}\end{array}\right] \tag{3}$$

$$\vec{E}_t^{\,II} = \sum_{m=0}^{M}\sum_{n=0}^{N}\left[\begin{array}{l}\left(B_{mn}^{h(+)}e^{-jk_{mn}^{II}z}\vec{e}_{t,mn}^{\,h(II)}\right. \\ -B_{mn}^{e(+)}e^{-jk_{mn}^{II}z}\vec{e}_{t,mn}^{\,e(II)} \\ +B_{mn}^{h(-)}e^{jk_{mn}^{II}(z-l)}\vec{e}_{t,mn}^{\,h(II)} \\ \left.+B_{mn}^{e(-)}e^{jk_{mn}^{II}(z-l)}\vec{e}_{t,mn}^{\,e(II)}\right)\end{array}\right] \tag{4}$$

$$\vec{H}_t^{\,II} = \sum_{m=0}^{M}\sum_{n=0}^{N}\left[\begin{array}{l}\left(-B_{mn}^{h(+)}e^{-jk_{mn}^{II}z}\vec{h}_{t,mn}^{\,h(II)}\right. \\ +B_{mn}^{e(+)}e^{-jk_{mn}^{II}z}\vec{h}_{t,mn}^{\,e(II)} \\ +B_{mn}^{h(-)}e^{jk_{mn}^{II}(z-l)}\vec{h}_{t,mn}^{\,h(II)} \\ \left.+B_{mn}^{e(-)}e^{jk_{mn}^{II}(z-l)}\vec{h}_{t,mn}^{\,e(II)}\right)\end{array}\right] \tag{5}$$

$$k_{mn}^{I} = \sqrt{\omega^2\mu_o\varepsilon_0 - \left(m\pi/A\right)^2 - \left(n\pi/B\right)^2} \tag{6}$$

$$k_{mn}^{II} = \sqrt{\omega^2\mu_o\varepsilon_0 - \left(m\pi/a\right)^2 - \left(n\pi/b\right)^2} \tag{7}$$

where
k is the mode propagation constant,
e^h is the normal *TE* mode vector,
h^h is the normal *TM* mode vector,
m and, n are mode indices,
E_t is the tangential electric field,
H_t is the tangential magnetic field.
For z=0 $\vec{E}_t^{\,II} = \vec{E}_t^{\,I}$

$$\begin{array}{l}(\delta_{mn,10}\vec{e}_{t,mn}^{\,h(I)} + A_{mn}^{h}\vec{e}_{t,mn}^{\,h(I)}) = \\ (B_{mn}^{h(+)}\vec{e}_{t,mn}^{\,h(II)} + B_{mn}^{h(-)}e^{-jk_{mn}^{II}l}\vec{e}_{t,mn}^{\,h(II)})\end{array} \tag{8}$$

$$(A_{mn}^{e}\vec{e}_{t,mn}^{\,e(I)}) = (-B_{mn}^{e(+)}\vec{e}_{t,mn}^{\,e(II)} + B_{mn}^{e(-)}e^{-jk_{mn}^{II}l}\vec{e}_{t,mn}^{\,e(II)}) \tag{9}$$

By finding the reflection coefficient in the second part, which is indicated with a minus sign, the equation below, which consists of the effects of the third and fourth parts, can be used as follows :

$$\Gamma_{23} = \frac{Z_3 - Z_{er}}{Z_3 + Z_{er}} \tag{10}$$

$$Z_3 = Z_0 \frac{e^{ik_{mn}^{II}d} - e^{-ik_{mn}^{II}d}}{e^{ik_{mn}^{II}d} + e^{-ik_{mn}^{II}d}} \tag{11}$$

$$\Gamma_{12} = \frac{Z_2 - Z_0}{Z_2 + Z_0} \tag{12}$$

$$Z_2 = Z_{er} \frac{e^{\gamma t} + \Gamma_{23} e^{-\gamma t}}{e^{\gamma t} - \Gamma_{23} e^{-\gamma t}} \tag{13}$$

$$Z_{mn}^h = \frac{\omega\mu}{k_{mn}^{II}} \; Z_{mn}^e = \frac{k_{mn}^{II}}{\omega\varepsilon} \tag{14}$$

$$\gamma = \sqrt{\left(m.\pi / a\right)^2 + \left(n.\pi / b\right)^2 - \omega^2 \mu_o \varepsilon_0 \varepsilon_r} \tag{15}$$

$$B_{mn}^- = B_{mn}^+ e^{-jk_{mn}^{II} l} \Gamma_{12} = B_{mn}^+ . \Gamma_0 \tag{16}$$

To enable the condition $z \times \left(\vec{H}_t^{II} - \vec{H}_t^{I} \right) = 0$ on the aperture (z=0 plane)

$$\sum_{m=0}^{M} \sum_{n=0}^{N} \left[\begin{array}{l} \left(B_{mn}^{h(+)} \vec{e}_{t,mn}^{\,h(II)} \right) \left(\begin{array}{l} \dfrac{1}{Z_{mn}^{h(II)}} + \dfrac{1}{Z_{mn}^{h(I)}} - \\ \Gamma_0 e^{-jk_{mn}^{II} l} \left(\dfrac{1}{Z_{mn}^{h(II)}} - \dfrac{1}{Z_{mn}^{h(I)}} \right) \end{array} \right) \\ -\left(B_{mn}^{e(+)} \vec{e}_{t,mn}^{\,e(II)} \right) \left(\begin{array}{l} \dfrac{1}{Z_{mn}^{e(II)}} + \dfrac{1}{Z_{mn}^{e(I)}} - \\ \Gamma_0 e^{-jk_{mn}^{II} l} \left(\dfrac{1}{Z_{mn}^{e(II)}} - \dfrac{1}{Z_{mn}^{e(I)}} \right) \end{array} \right) \end{array} \right] = 2\delta_{10} \frac{1}{Z_{10}^{h(I)}} e_{10}^{h(I)} \tag{17}$$

We can write the approximate magnetic current as follows:

$$\left(\delta_{mn,10} + A_{mn}^h \right) = \int_{S_a} \vec{M}_s . \left(\hat{z} \times \vec{e}_{t,mn}^{\,h} \right) ds \tag{18}$$

$$A_{mn}^e = \int_{S_a} \vec{M}_S . \left(\hat{z} \times \vec{e}_{t,mn}^{\,e} \right) ds \tag{19}$$

$$B_{mn}^{h(+)} = \frac{1}{1 + \Gamma_0 e^{-jk_{mn}^{II} l}} \int_{S_a} \vec{M}_S . \left(\hat{z} \times \vec{e}_{t,mn}^{\,h} \right) ds \tag{20}$$

$$B_{mn}^{e(+)} = \frac{1}{-1 + \Gamma_0 e^{-jk_{mn}^{II} l}} \int_{S_a} \vec{M}_S . \left(\hat{z} \times \vec{e}_{t,mn}^{\,e} \right) ds \tag{21}$$

The magnetic current is approximated with a truncated set of independent basis functions:

$$\bar{M}_s(\vec{\rho}\,') \cong \sum_{p}^{P}\left[a_{p_x} u_{p_x}(\vec{\rho}\,')\hat{x} + a_{p_y} u_{py}(\vec{\rho}\,')\hat{y} \right] \tag{22}$$

$$(\delta_{mn,10} + A^h_{mn}) = \sum_{m=0}^{M}\sum_{n=0}^{N}\int_{S_a}\left(- a_{mnx} u_{mnx} e^h_{y,mn} + a_{mny} u_{mny} e^h_{x,mn}\right)ds \tag{23}$$

$$A^e_{mn} = \sum_{m=0}^{M}\sum_{n=0}^{N}\int_{S_a}\left(-a_{mnx} u_{mnx} e^e_{y,mn} + a_{mny} u_{mny} e^e_{x,mn}\right)ds \tag{24}$$

$$\begin{aligned} B^{h(+)}_{mn} + B^{h(-)}_{mn}.e^{-jk^{II}_{mn}l} &= \sum_{m=0}^{M}\sum_{n=0}^{N}\int_{S_a}\left(- a_{mnx} u_{mnx} e^h_{y,mn} + a_{mny} u_{mny} e^h_{x,mn}\right)ds \\ - B^{e(+)}_{mn} + B^{e(-)}_{mn}.e^{-jk^{II}_{mn}l} &= \sum_{m=0}^{M}\sum_{n=0}^{N}\int_{S_a}\left(- a_{mnx} u_{mnx} e^e_{y,mn} + a_{mny} u_{mny} e^e_{x,mn}\right)ds \end{aligned} \tag{25}$$

$$\begin{bmatrix} B^{h(+)}_{mn} \\ B^{e(+)}_{mn} \end{bmatrix} = \begin{bmatrix} 1+\Gamma_0.e^{-jk^{II}_{mn}l} & 0 \\ 0 & -1+\Gamma_0.e^{-jk^{II}_{mn}l} \end{bmatrix}^{-1} \begin{bmatrix} -\int_{S_a} u_{mnx} e^h_{y,mn} ds & \int_{S_a} u_{mny} e^h_{x,mn} ds \\ -\int_{S_a} u_{mnx} e^e_{y,mn} ds & \int_{S_a} u_{mny} e^e_{x,mn} ds \end{bmatrix} \begin{bmatrix} a_{mnx} \\ a_{mny} \end{bmatrix} \tag{26}$$

$$\begin{bmatrix} \left(\frac{1}{Z^{h(II)}_{mn}} + \frac{1}{Z^{h(I)}_{mn}} - \Gamma_0.e^{-jk^{II}_{mn}l}\left(\frac{1}{Z^{h(II)}_{mn}} - \frac{1}{Z^{h(I)}_{mn}}\right)\right)\int_{S_a} w_{sx}\,\vec{e}^{\,h(II)}_{mn}\,ds & -\left(\frac{1}{Z^{e(II)}_{mn}} + \frac{1}{Z^{e(I)}_{mn}} - \Gamma_0.e^{-jk^{II}_{mn}l}\left(\frac{1}{Z^{e(II)}_{mn}} - \frac{1}{Z^{e(I)}_{mn}}\right)\right)\int_{S_a} w_{sy}\,\vec{e}^{\,e(II)}_{mn}\,ds \\ \left(\frac{1}{Z^{h(II)}_{mn}} + \frac{1}{Z^{h(I)}_{mn}} - \Gamma_0.e^{-jk^{II}_{mn}l}\left(\frac{1}{Z^{h(II)}_{mn}} - \frac{1}{Z^{h(I)}_{mn}}\right)\right)\int_{S_a} w_{sx}\,\vec{e}^{\,h(II)}_{mn}\,ds & -\left(\frac{1}{Z^{e(II)}_{mn}} + \frac{1}{Z^{e(I)}_{mn}} - \Gamma_0.e^{-jk^{II}_{mn}d}\left(\frac{1}{Z^{e(II)}_{mn}} - \frac{1}{Z^{e(I)}_{mn}}\right)\right)\int_{S_a} w_{sy}\,\vec{e}^{\,e(II)}_{mn}\,ds \end{bmatrix}$$

$$\cdot \begin{bmatrix} 1+\Gamma_0.e^{-j\,k^{II}_{mn}l} & 0 \\ 0 & -1+\Gamma_0.e^{-j\,k^{II}_{mn}l} \end{bmatrix}^{-1} \begin{bmatrix} -\int_{S_a} u_{mnx} e^h_{y,mn} ds & \int_{S_a} u_{mny} e^h_{x,mn} ds \\ -\int_{S_a} u_{mnx} e^e_{y,mn} ds & \int_{S_a} u_{mny} e^e_{x,mn} ds \end{bmatrix} \begin{bmatrix} a_{mnx} \\ a_{mny} \end{bmatrix} = \begin{bmatrix} \frac{2}{Z^{h(I)}_{10}}\int_{S_a} w_{sx}\,\vec{e}^{\,h(I)}_{x10}\,ds \\ \frac{2}{Z^{h(I)}_{10}}\int_{S_a} w_{sy}\,\vec{e}^{\,h(I)}_{y10}\,ds \end{bmatrix} \tag{27}$$

By solving the above matrix equation, it is possible to determine the a_{mnx} and a_{mny} coefficients. The B coefficients can be obtained by means of (26).

On the condition that the waveguide is between c_1 and c_2 in the x direction and between v_1 and v_2 in the y direction the base and weighting functions can be presented as follows (Terril, 1998):

$$\begin{aligned} u_{mnx} &= \sin\left(\frac{p\pi(x-c_1)}{c}\right)\cos\left(\frac{q\pi(y-v_1)}{v}\right) \\ w_{sx} &= \cos\left(\frac{s\pi(x-c_1)}{c}\right)\sin\left(\frac{t\pi(y-v_1)}{v}\right) \\ u_{mny} &= \cos\left(\frac{p\pi(x-c_1)}{c}\right)\sin\left(\frac{q\pi(y-v_1)}{v}\right) \\ w_{sy} &= \sin\left(\frac{s\pi(x-c_1)}{c}\right)\cos\left(\frac{t\pi(y-v_1)}{v}\right) \end{aligned} \tag{28}$$

3. NUMERICAL RESULTS

In this study, the amplitude of the reflection coefficient according to the change in material thickness was found in relation to the different positions of the material within the resonator. The results obtained with the mode matching method were compared with the results obtained through Ansoft HFSS. The variations in the reflection coefficient were determined by changing the material thickness within the range of 10 mm and 85 mm for different material positions. While the dielectric constant of the material was taken as 4.17-1.55i, the dimensions of the resonator were taken as 378 mm along the x axis, 258 mm along the y axis and 325 mm along the z axis.

Examining Figure 2 reveals that, for a height of d=60 mm, the minimum reflection coefficient value is obtained when the material thickness is t=80 mm. Material thicknesses of t=20 mm and t=40 mm are the other thickness values that result in low reflection coefficients.

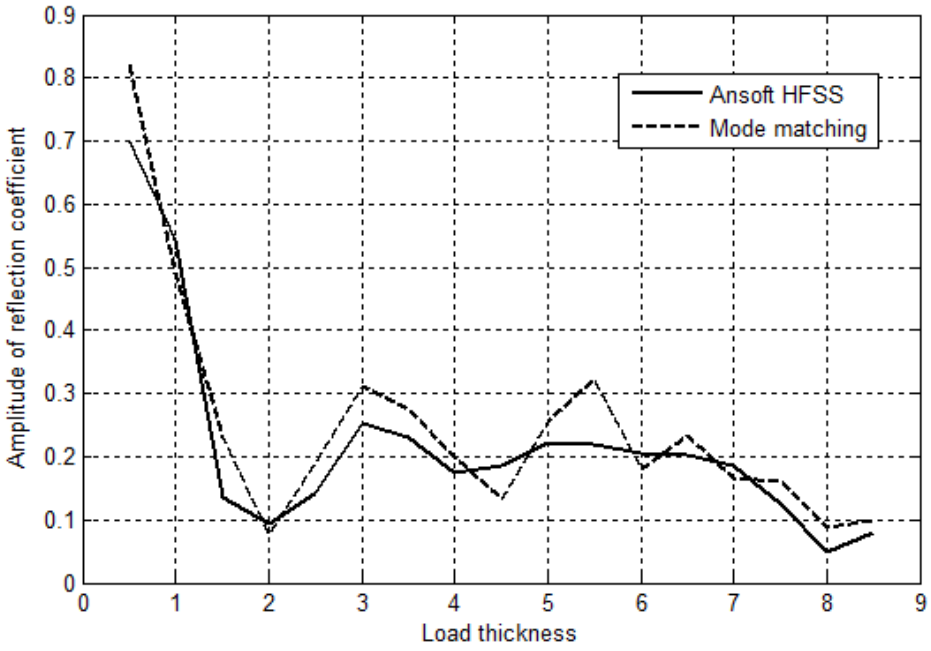

Figure 2:
Reflection coefficient variation according to the material thickness for d=60 mm

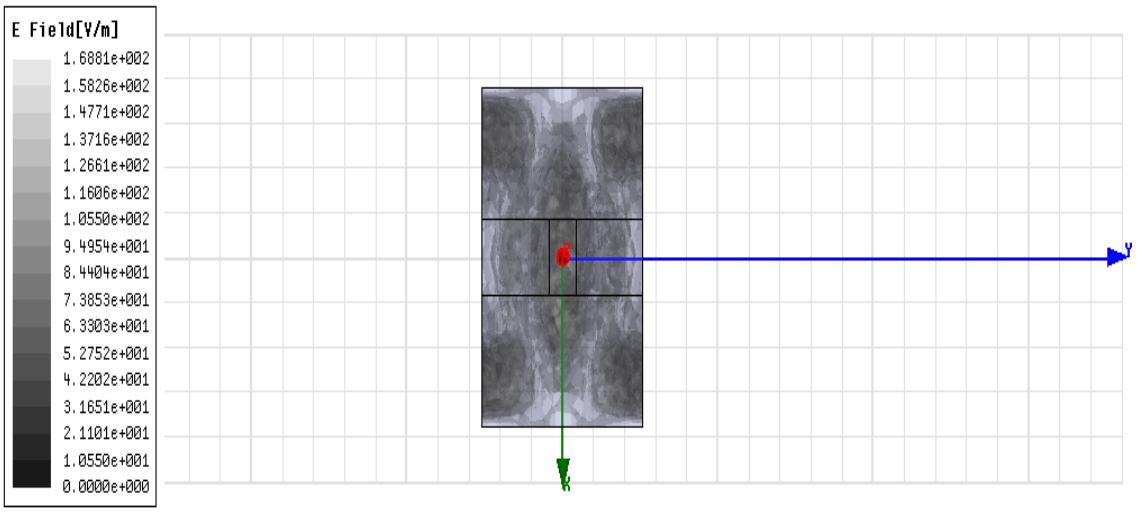

Figure 3:
Top view of the electric field distribution on the material when the material is 80 mm thick for d=60 mm

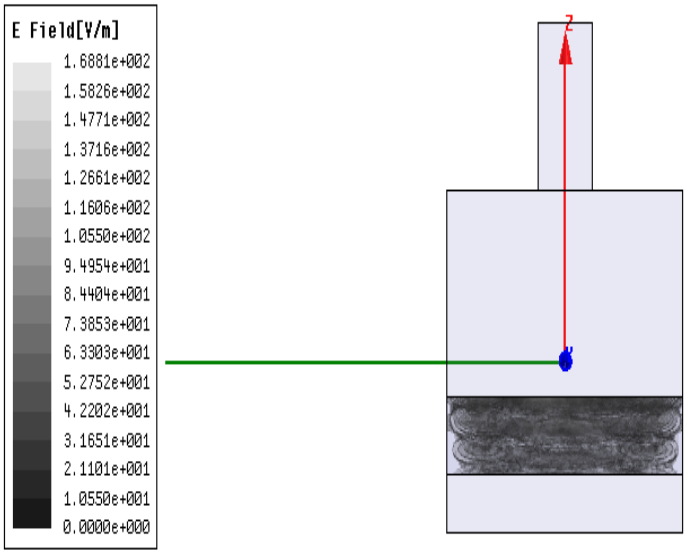

Figure 4:
Sectional view of the electric field distribution on the material when the material is 80 mm thick for d=60 mm

Examining the electric field distributions in Figures 3 and 4 shows that because the thickness of the material is large, the power had only a slight effect on the material.

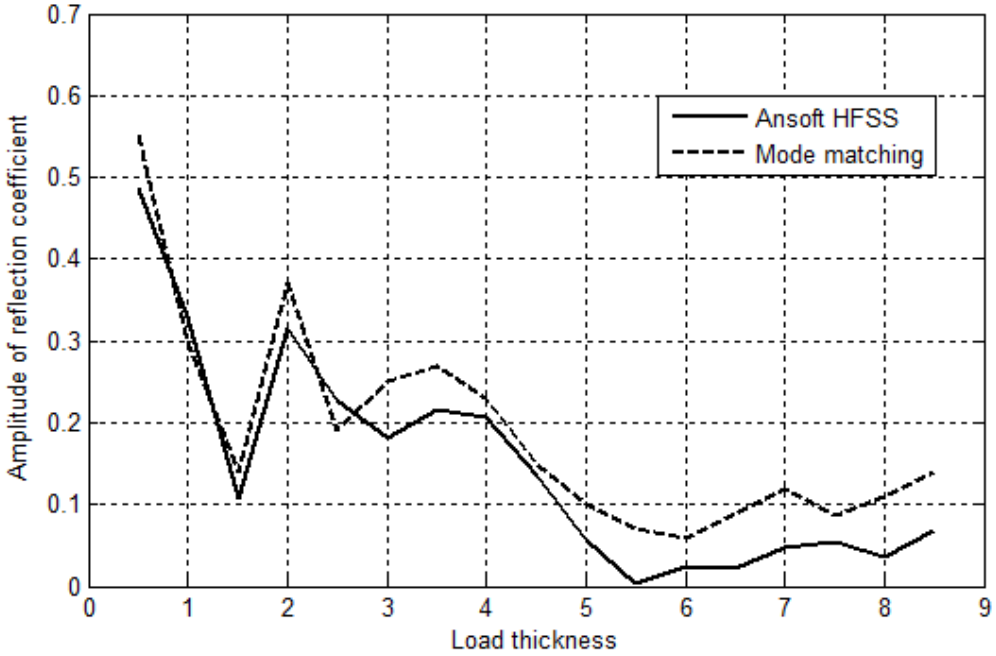

Figure 5:

Reflection coefficient variation according to the material thickness for d=120 mm

Figure 5 shows that at a height value of d=120 mm, the lowest reflection coefficient is obtained when the material thickness is t=55 mm; t=60 mm and t=65 mm are the other two material thickness values that resulted in low reflection coefficients.

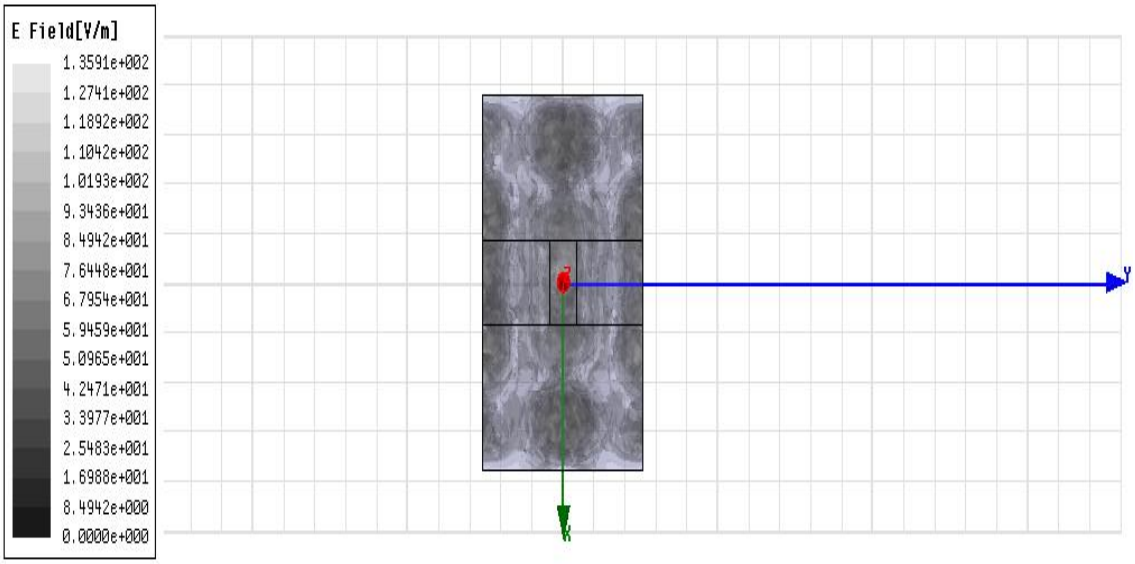

Figure 6:

Top view of the electric field distribution on the material when the material is 55 mm thick for d=120 mm

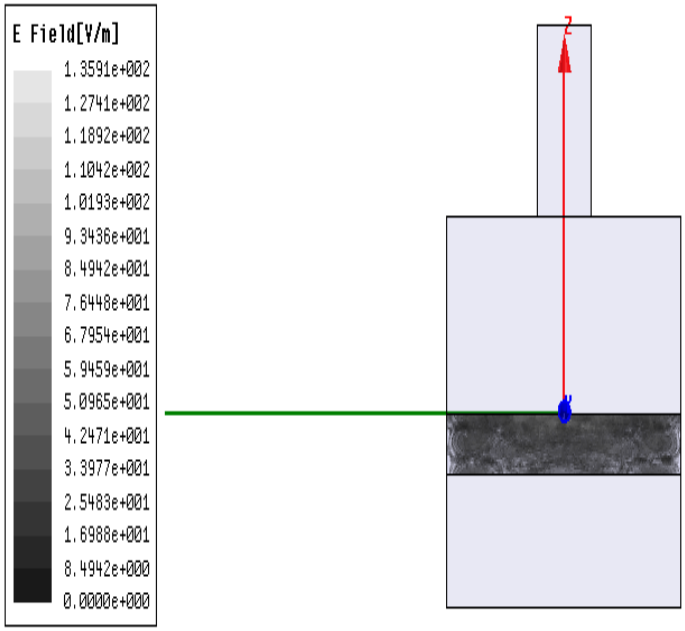

Figure 7:
Sectional view of the electric field distribution on the material when the material is 55 mm thick for d=120 mm

Examining Figures 6 and 7 show that the electric field distribution is not homogenous and local.

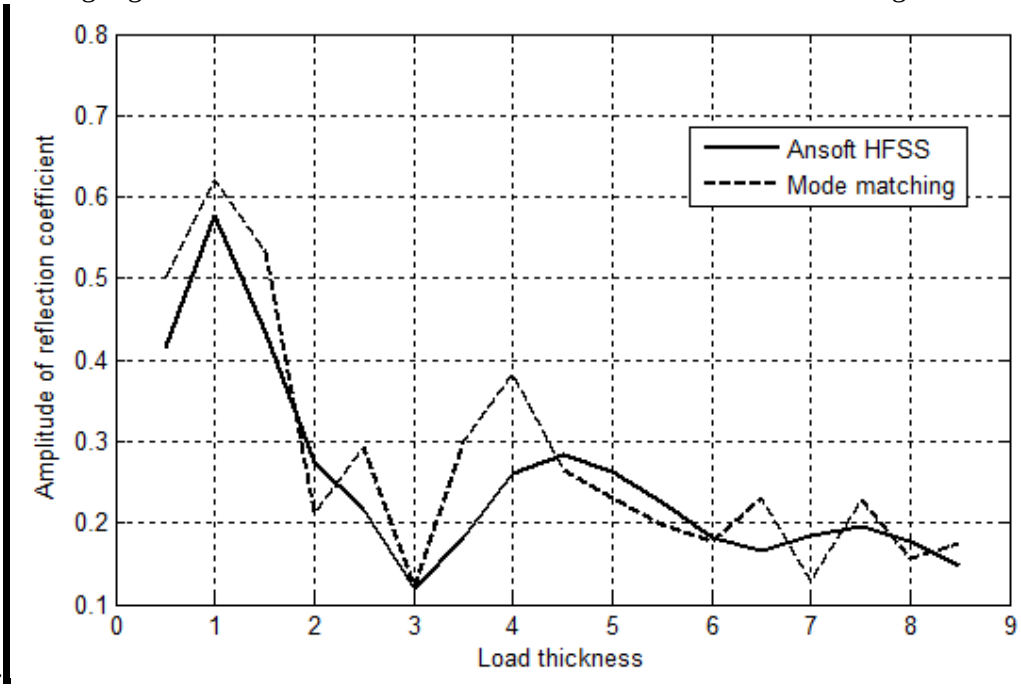

Figure 8:
Reflection coefficient variation according to material the thickness for d=180 mm

From Figure 8, it can be observed that, at a height of d=180 mm, the reflection coefficient exhibits the lowest value when the material thickness is t=30 mm; t=60 mm and t=85 mm are the other two material thickness values that resulted in low reflection coefficients.

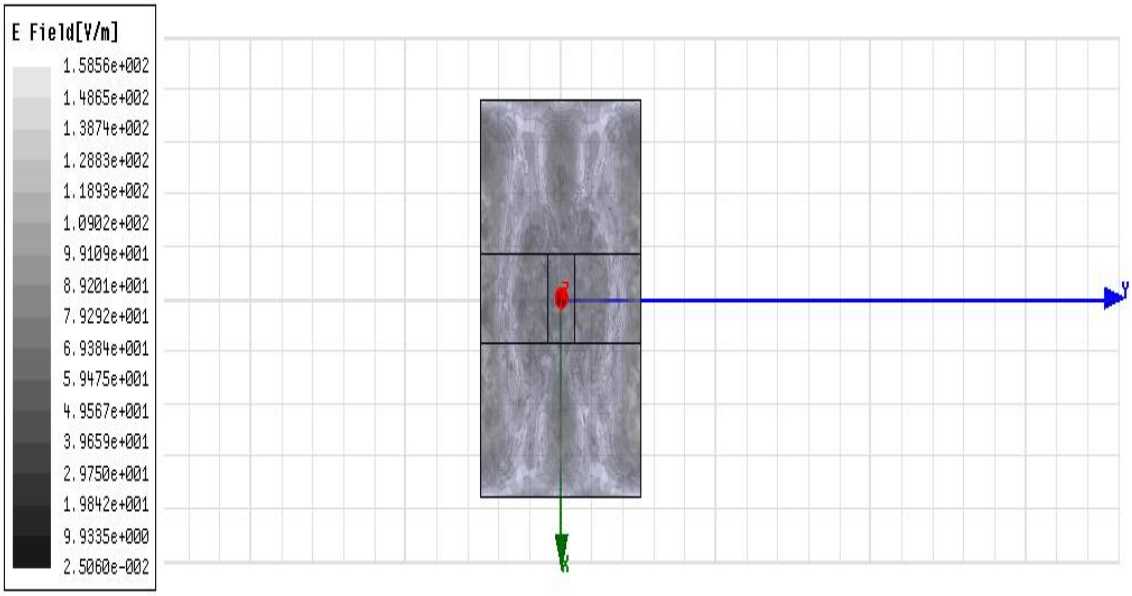

Figure 9:
Top view of the electric field distribution on the material when the material is 30 mm thick for d=180 mm

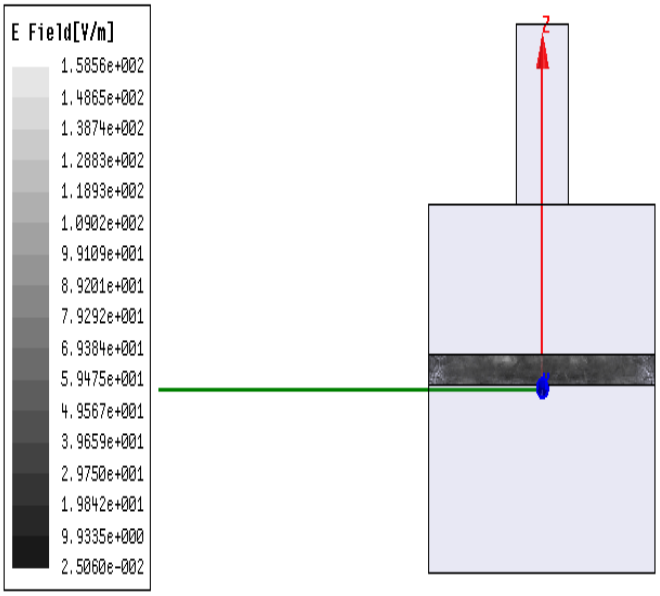

Figure 10:
Sectional view of the electric field distribution on the material when the material is 30 mm thick for d=180 mm.

Figures 9 and 10 show that the electric field distribution affected a much wider area. It affected the inside of the material in the same way.

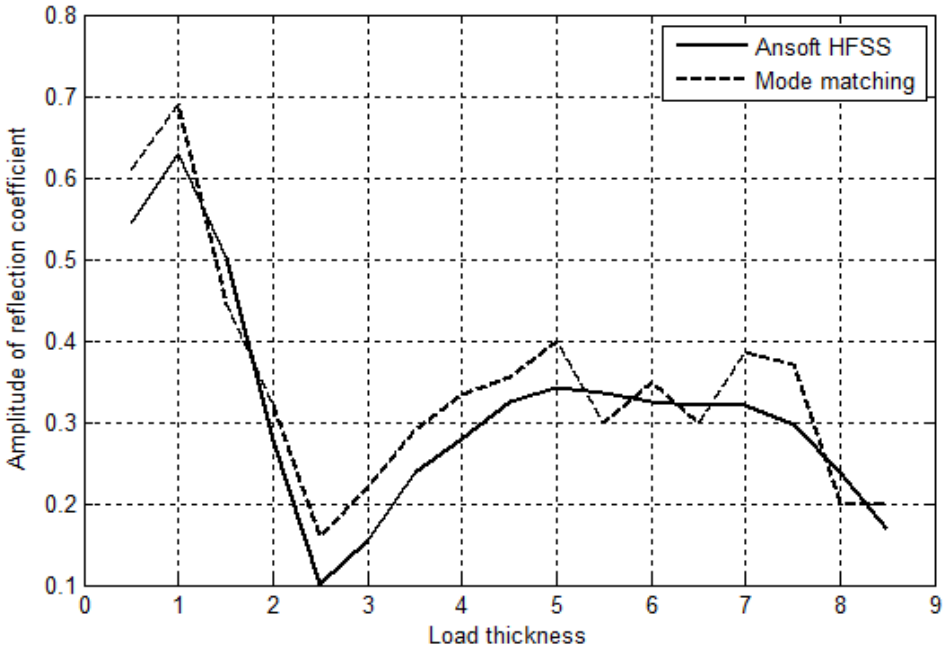

Figure 11:
Reflection coefficient variation according to the material thickness for d=240 mm

Figure 11 shows that, at a height of d=240 mm, the lowest reflection coefficient is obtained when the material thickness is t=25 mm; t=30 mm and t=85 mm are the other material thickness values that resulted in low reflection coefficients.

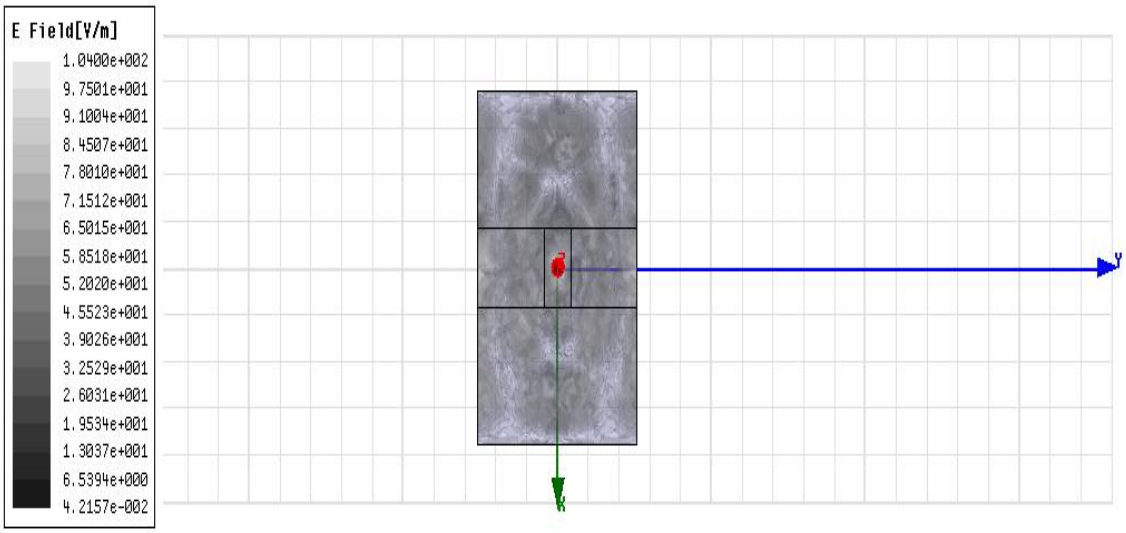

Figure 12:
Top view of the electric field distribution on the material when the material is 25 mm thick for d=240 mm

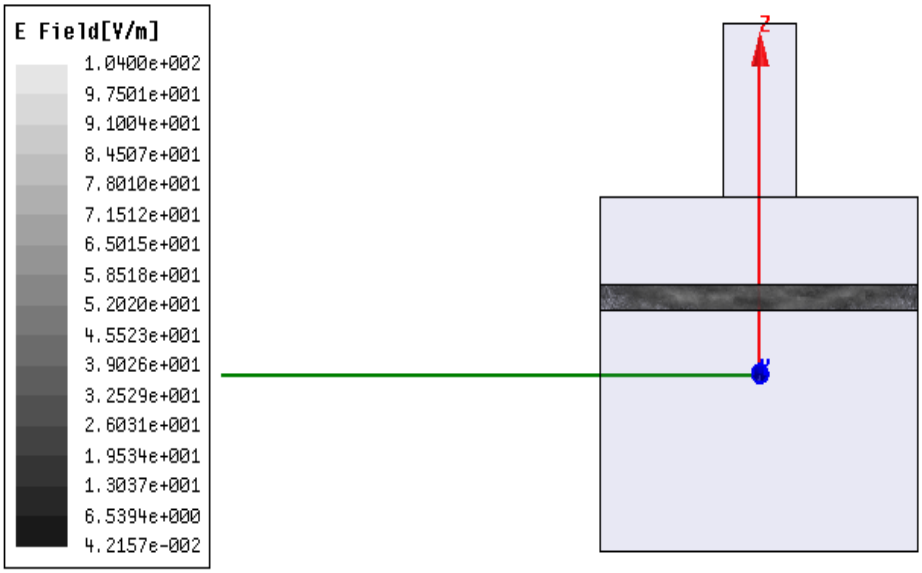

Figure 13:
Sectional view of the electric field distribution on the material when the material is 25 mm thick for d=240 mm

Figures 12 and 13 show that that the electric field is distributed in a nearly homogenous way on the surface of the material. It is also distributed within the material in an effective way.

Giving the reflection coefficient changes according to material thickness, figure 2, figure 5, figure 8 and figure 11 to obtain the sixty-eight different modeling was made by Ansoft HFSS. The method presented in this article, the reflection coefficient changes according to material thickness, with a single modeling, in a much shorter time and with high accuracy was obtained.

4. CONCLUSIONS

The objective in microwave heating is to uniformly distribute the field change on the material to be heated over as wide of an area as possible. In this way, homogenous heating can be achieved. A low reflection coefficient means that the power reflecting to the feed will be low. However, a low reflection coefficient does not necessarily mean that all the power will interact with the material to be heated. For instance, at a value that gives a low reflection coefficient, the power may be stored within the resonator. Nevertheless, to increase power efficiency within the oven, the material has to be placed at the position where the reflection coefficient is low. Doing so increases the possibility of the power interacting with the material.

The conclusions presented below are reached by examining the figures showing the electric field variation:

When the material is positioned at a height of d=120 mm from the base of the resonator, the reflection coefficient is s_{11}=0.0046 when the material thickness is t=55 mm. This indicates a power efficiency of 99.997 %. However, when the field changes on the material are examined, it is observed that the electric field affected the surface of the material as a hot point, and there was no significant effect within the material itself. This means that the electric field is mainly stored within the resonator.

When the material is positioned at a height of d=240 mm from the base of the resonator, the reflection coefficient is s_{11}=0.1004 when the material thickness is t=25 mm. According to the formula $p=1-(s_{11})^2$, there is 98.991 % power efficiency. Examining the area changes on the material revealed that the electric field uniformly affected a wide area at the top of the material. The power was also effectively distributed within the material.

Considering all of these data, it is possible to assert that the reflection coefficient variations obtained by alternating the position and the thickness of the material by means of a mode matching system is the first and the most important design phase for microwave ovens. By examining the field changes at the values for which the reflection coefficient is low, the position where the material will be placed within the resonator and the thickness of the material can be determined with a few electric field analyses.

REFERENCES

1. Dibben, D.C. and Metaxas, A.C. (1996) Time domain finite element analysis of multimode microwave applicators loaded with low and high loss materials, *IEEE Microwave and Guided Letters*, 32, 945-948.

2. Hallac A. and Metaxas A.C. (2003) Finite element time domainanalysis of microwave heating applicators using higher order vector finite elements, *International Conference on Microwave and High Frequency Heating, UK*, 21-25.

3. Iskander, M.F., Smith, R.L., Octavio, A., Andrade, M., Kimrey, H. and Walsh, L.M. (1994) FDTD simulation of microwave sintering of ceramics in multimode cavities, *IEEE Transactions on Microwave Theory and Tecniques*, 42(5), 1686-1689. doi: 10.1109/22.293527

4. Jia, X. (1993) Experimental and numerical study of microwave heating applicator, *Journal of Microwave Power and Elecromagnetic Energy*, 28 (1), 25-31.

5. Liu, F., Turner I. and Bialkowski, M. A. (1994) A Finite difference time domain simulation of power density distribution in a dielectric loaded microwave cavity, *Journal of Microwave Power and Electromagnetic Energy*, 29(3), 138-148.

6. Liu, F., Turner, I., Siores, E. and Groombridge, P. (1996) A numerical and experimental investigation of the microwave heating of polymer materials inside a ridge waveguide, *Journal of Microwave Power and Electromagnetic Energy*, 31(2), 71-82.

7. Monzo-Cabrera, J., Diaz-Morcillo, A., Pedreno-Molina, J. L. and Sanchez-Hernandez, D. (2004) A new method for load matching in multimode-microwave heating applicators based on the use of dielectric-layer superposition, *Microwave and Optıcal Technology Letters*, 40(4), 318-322. doi: 10.1002/mop.11367

8. Monzo-Cabrera, J., Escalante, J., Dıaz-Morcillo, A., Martınez-Gonzalez, A. and Sanchez-Hernandez, D. (2004) Load matching in multimode microwave-heating applicators based on the use of dielectric layer moulding with commercial materials, *Microwave and Optical Technology Letters*, 41(5), 414-417. doi: 10.1002/mop.20156

9. Pedreno-Molina, J. L., Monzo-Cabrera, J. and Catala–Civera, J. M. (2006) Sample movement optimization for uniform heating in microwave heating ovens, *International Journal of RF and Microwave Computer-Aided Engineering*, 142-152. doi: 10.1002/mmce.20208

10. Plaza-González, P., Monzó-Cabrera, J., Catalá-Civera, J. M. and Sánchez-Hernández, D. (2004) New approach for the prediction of the electric field distribution in multimode microwave-heating applicators with mode stirrers, *IEEE Transactions on Magnetics*, 40(3), 1672-1678. doi:10.1109/TMAG.2003.821560

11. Plaza-González, P., Monzó-Cabrera, J., Catalá-Civera, J. M., and Sánchez-Hernández, D. (2005) Effect of mode-stirrer configurations on dielectric heating performance in multimode microwave applicators, *IEEE Transactions on Microwave Theory and Techniques*, 53(5), 1699-1706. doi:10.1109/TMTT.2005.847066

12. Reader, H.C. and Chow Ting Chan, T.V. (1998) Experimental and numerical field studies in loaded multimode and single mode cavities, *Journal of Microwave Power and Elecromagnetic Energy*, 33(2), 256-263.

13. Requena-Perez, M. E., Pedreno-Molina, J. L., Pinzolas-Prado, M., Monzo-Cabrera, J., Diaz-Morcillo, A. and Sanchez-Hernandez, D. (2004) Load matching in multimode microwave-heating applicators by load location optimization, *34" European Microwave Conference, Amsterdam, Holland.*

14. Süle, O. and Kent, S. (2010) Analysis of microwave cavity loaded with lossy dielectric slab by means of mode matching method and optimization of load location', *PIER M*, 14, 71-83. doi:10.2528/PIERM10061707

15. Sunberg, M., Risman, P.O., Kildal, P.S. and Ohlsson, T. (1996) Analysis and design of industrial microwave ovens using the finite difference time domain method, *Journal of Microwave Power and Elecromagnetic Energy*, 31(3), 142-157.

16. Terril, N. D. (1998) Field simulation for the microwave heating of thin ceramic fibers. *MSc. thesis,* State University.

17. Zhao, H. and Turner, I.W. (1996) An analysis of the finite difference time domain method for modelling the microwave heating of dielectric materials within a three dimensional cavity system, *Journal of Microwave Power and Electromagnetic Energy*, 31(4), 199-214.